First-Principles Investigation of Phase Stability in the O2-LiCoO2 System

4 **AUTHORS**, INCLUDING:

Dany Carlier
Institut de Chimie de la matière condensée d…

98 PUBLICATIONS **1,505** CITATIONS

SEE PROFILE

Gerbrand Ceder
University of California, Berkeley

502 PUBLICATIONS **20,991** CITATIONS

SEE PROFILE

First-Principles Investigation of Phase Stability in the O2-LiCoO$_2$ System

D. Carlier,[†,‡] A. Van der Ven,[†] C. Delmas,[‡] and G. Ceder*,[†]

Department of Materials Science and Engineering, Massachusetts Institute of Technology, 77 Massachusetts Avenue, Cambridge, Massachusetts 02139, and Institut de Chimie de la Matière Condensée de Bordeaux−CNRS and Ecole Nationale Supérieure de Chimie et Physique de Bordeaux, Université Bordeaux I, 87 Avenue du Dr. A. Schweitzer, 33608 Pessac Cedex, France

A first-principles investigation of the phase stability in the O2-LiCoO$_2$ system is performed to better understand the unusual layered phases obtained upon Li deintercalation (i.e., T$^\#$2 and O6). First-principles pseudopotential calculations within the local density approximation and thermodynamic models extracted from these calculations both show that two tetrahedral sites for the Li ions need to be considered in the T$^\#$2 structure for qualitative agreement with experiment to be obtained. Only when both tetrahedral sites in T$^\#$2 are considered is the experimentally observed two-phase O2/T$^\#$2 region predicted. This indicates that this structural phase transformation is induced by enhanced configurational entropy in the T$^\#$2 phase and not by a metal−insulator transition as was previously proposed. We also predict that two ordered compounds are stable at room temperature: Li$_{1/4}$CoO$_2$ in the O2 structure and Li$_{1/3}$CoO$_2$ in the O6 structure. We show that the formation of the O6 phase is not related to Li staging.

1. Introduction

LiCoO$_2$ can exhibit two types of layered structures: O3 and O2. The thermodynamically stable structure is prepared by solid-state reaction and exhibits an O3 stacking where the LiO$_6$ and CoO$_6$ octahedra share only edges. The O2-type LiCoO$_2$ is metastable and was prepared for the first time by Delmas et al. by Na$^+$/Li$^+$ exchange from the P2−Na$_{0.70}$CoO$_2$ phase.[1] In this structure, the LiO$_6$ octahedra share edges but also faces with the CoO$_6$ octahedra. Recently, some of us reinvestigated O2-LiCoO$_2$ from the structural point of view.[2] Rietveld refinement of the neutron diffraction pattern indicated that the repulsion between the lithium and cobalt ions through the common face of their octahedra is strong enough to displace them from the center of their octahedra.[2]

Whereas O3-LiCoO$_2$ has been extensively studied as a positive electrode in lithium batteries,[3−7] to our knowledge, very few papers have dealt with the

O2- LiCoO$_2$ system.[8−10] Paulsen at al. showed that the O2-LiCoO$_2$ electrochemical properties for battery applications compete with those of the conventional O3-LiCoO$_2$, and DSC measurements indicate that the O2-Li$_x$CoO$_2$ system charged up to 4.2 V is about as safe as the O3 material at the same potential.[9] During lithium deintercalation, the O2 system exhibits several reversible voltage plateaus (Figure 1) that are associated with phase transformations involving either CoO$_2$ sheet gliding or lithium/vacancy ordering. Several unusual structures in layered oxides are observed: T$^\#$2, T$^\#$2′, and O6.[10] All of these phases are named following the packing designation proposed previously by Delmas et al. for the layered oxides: the P, T, or O letter describes the alkali ion site (prismatic, tetrahedral, or octahedral, respectively) and the number 1, 2, 3, ..., indicates the number of slabs within the hexagonal cell.[11] The # symbol was used for the T$^\#$2 phase, which is stable for 0.52 < x ≤ 0.72, because this phase exhibits a new oxygen stacking in which the oxygen ions do not occupy the positions of the same triangular lattice.

The formation of the T$^\#$2 structure from the O2 structure requires every other CoO$_2$ slab to glide by ($^1/_3$, $^1/_6$, 0), yielding an orthorhombic cell in the *Cmca* space group. This stacking was recently observed, for the first time, in Li$_{2/3}$Ni$_{1/3}$Mn$_{2/3}$O$_2$ by Dahn et al.[12,13] Three types of distorted tetrahedral sites are available in the T$^\#$2

---

* Corresponding author. Tel.: 1-617-253-1581. Fax: 1-617-258-6534. E-mail address: gceder@mit.edu.
　† Massachusetts Institute of Technology.
　‡ Institut de Chimie de la Matière Condensée de Bordeaux
　(1) Delmas, C.; Braconnier, J. J.; Hagenmuller, P. *Mater. Res. Bull.* **1982,** *17,* 117.
　(2) Carlier, D.; Saadoune, I.; Suard, E.; Croguennec, L.; Ménétrier, M.; Delmas, C. *Solid State Ionics* **2001,** *144,* 263.
　(3) Mizushima, K.; Jones, P. C.; Wiseman, P. J.; Goodenough, J. B. *Mater. Res. Bull.* **1980,** *15,* 783.
　(4) Reimers, J. N.; Dahn, J. R. *J. Electrochem. Soc.* **1992,** *139* (8), 2091.
　(5) Ohzuku, T.; Ueda, A. *J. Electrochem. Soc.* **1994,** *141* (11), 2972.
　(6) Amatucci, G. G.; Tarascon, J. M.; Klein, L. C. *J. Electrochem. Soc.* **1996,** *143* (3), 1114.
　(7) Ménétrier, M.; Saadoune, I.; Levasseur, S.; Delmas, C. *J. Mater. Chem.* **1999,** *9,* 1135.

　(8) Mendiboure, A.; Delmas, C.; Hagenmuller, P. *Mater. Res. Bull.* **1984,** *19,* 1383.
　(9) Paulsen, J. M.; Mueller-Neuhaus, J. R.; Dahn, J. R. *J. Electrochem. Soc.* **2000,** *147* (2), 508.
　(10) Carlier, D.; Saadoune, I.; Ménétrier, M.; Delmas, C. *J. Electrochem. Soc.* **2002,** *149* (10), A1310.
　(11) Delmas, C.; Fouassier, C.; Hagenmuller, P. *Physica B* **1980,** *99,* 81.
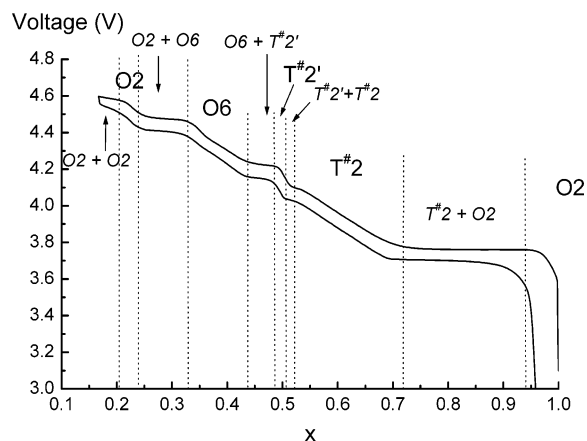
Figure 1. Voltage curve of a Li//O2-LiCoO₂ cell obtained with a C/40 current density rate (40 h is needed to extract one Li per formula unit). The higher and lower curves represent Li removal and insertion, respectively.

structure for Li occupation: 8e, 8f$_{edges}$, and 8f$_{face}$.[10,14] In their neutron diffraction analyses of the T#2-LiNi$_{1/3}$Mn$_{2/3}$O$_2$ phase, Paulsen et al. placed the Li ions in the 8e sites, but did not consider other possibilities.[12] In the T#2-Li$_x$CoO$_2$ phase, the lithium ions were shown to be situated preferentially in the 8e sites, but some nuclear density was also found in the 8f$_{edges}$ sites, in good agreement with our first-principles investigation of the relative stability of the sites.[14] In their study of the Li$_{2/3}$Ni$_{1/3}$Mn$_{2/3}$O$_2$ phase, Paulsen et al. reported that Ni/Mn ordering in the slabs was essential for the T#2 formation. However, in the O2-LiCoO$_2$ system, the T#2 phase is stabilized around the same Li concentration, and no charge ordering Co^{3+}/Co^{4+} is expected, as this phase is metallic.[10] More recently, Dahn's group reported the formation of the T#2 structure for Li$_{2/3}$Co$_{2/3}$Mn$_{1/3}$O$_2$, which does not exhibit Co/Mn ordering.[15] Hence, cation ordering might not be crucial in the formation of T#2, and the reasons for the stability of this structure remain unclear.

Some of us recently investigated the possibility of lithium/vacancy ordering in T#2-Li$_x$CoO$_2$ by neutron powder diffraction analyses and electron diffraction.[14,16] Whereas no Li/vacancy ordering was evidenced in the neutron scattering data, the electron diffraction study revealed that, actually, the large T#2 domain corresponds not to a single phase but to a series of complex structures with several Li/vacancy orderings.[16] Further lithium deintercalation from T#2-Li$_x$CoO$_2$ leads to a T#2'- Li$_x$CoO$_2$ phase that exhibits a very narrow concentration domain situated around $x = 0.5$ (Figure 1). This phase is thought to exhibit a lithium/vacancy ordering similar to that observed in the O3-LiCoO$_2$ system,[4,17] but no direct evidence of it has been reported

so far. Moreover, its XRD pattern is similar to that of the T#2-Li$_x$CoO$_2$ phases.[9,10]

Further lithium deintercalation leads to the O6 phase ($0.33 \leq x < 0.42$), which was first characterized by XRD by Mendiboure et al.[8] This stacking exhibits two types of CoO$_2$ layers, and the possibility of Co^{3+}/Co^{4+} ordering over these layers has been inferred from XRD Rietveld refinement.[10]

For lower lithium concentrations, the O2 stacking is again stabilized, and two phases were found: one stable for $0.21 \leq x < 0.25$[9,10] and a second one for $x < 0.18$.[10]

The O2-LiCoO$_2$ system is very interesting from a fundamental point of view, as it exhibits several phase transformations upon lithium deintercalation that lead to unusual structures that are not fully characterized. Therefore, to better understand these structures and the driving forces responsible for the phase transformations involved in lithium deintercalation, we have performed a first-principles study of the phase diagram of the layered Li$_x$CoO$_2$ phases derived from O2-LiCoO$_2$. It has been demonstrated that information about phase stability can be obtained through a combination of accurate first-principles total-energy calculations and statistical-mechanics techniques such as Monte Carlo simulations.[18–20] Such a method has already been applied to investigate the phase diagram of the layered Li$_x$CoO$_2$ phases derived from O3-LiCoO$_2$[21–25] and, more recently, the phase diagram of the Li$_x$NiO$_2$ system.[26]

In this paper, we first give a short description of the method used (section 2) and then present the three host structures chosen for the phase diagram simulation (O2, T#2, and O6) (section 3.1). The relative stability of the three hosts as a function of Li concentration at 0 K is discussed in section 3.2. The resulting calculated phase diagram is presented in section 3.4. The results are discussed and compared to experiments in section 3.5. Finally, in section 4, we discuss the driving forces for the phase transformations.

2. Method

A detailed theoretical background for obtaining a phase diagram from first-principles calculations can be found in some of our previous papers.[24,25] Essentially, the approach consists of using first-principles calculations to parametrize the energy as a function of occupation variables assigned to each possible Li site. Such a parametrization can then be used to calculate the energy of any Li/vacancy arrangement within a given host. The parametrization takes the form of a generalized lattice model Hamiltonian (the cluster expansion). The interactions in this expansion are determined by fitting to the first-principles calculated energy of a large number of Li/vacancy configurations. A separate cluster expansion needs to be constructed for each of the O2, O6, and T#2 hosts. Using Monte Carlo simulations, stable ordering in each host and free energies as a function of lithium concentration and tempera-

(12) Paulsen, J. M.; Donaberger, R. A.; Dahn, J. R. *Chem. Mater.* **2000**, *12*, 2257.
(13) Paulsen, J. M.; Dahn, J. R. *J. Electrochem. Soc.* **2000**, *147* (7), 2478.
(14) Carlier, D.; Croguennec, L.; Ceder, G.; Ménétrier, M.; Shao-Horn, Y.; Delmas, C. *Inorg. Chem.*, manuscript submitted.
(15) Lu, Z.; Donaberger, R. A.; Thomas, C. L.; Dahn, J. R. *J. Electrochem. Soc.* **2002**, *149* (8), A1083.
(16) Shao-Horn, Y.; Croguennec, L.; Carlier, D.; Weill, F.; Ménétrier, M.; Delmas, C. *Chem. Mater.*, manuscript submitted.
(17) Shao-Horn, Y.; Levasseur, S.; Weill, F.; Delmas, C. *J. Electrochem. Soc.*, manuscript submitted.

(18) De Fontaine, D. *Solid State Physics*; Academic Press: New York, 1994.
(19) Ceder, G.; Kohan, A. F.; Aydinol, M. K.; Tepesch, P. D.; Van der Ven, A. *J. Am. Ceram. Soc.* **1998**, *81* (3), 517.
(20) Zunger, A. *Statistics and Dynamics of Alloy Phase Transformations*; Plenum Press: New York, 1994.
(21) Wolverton, C.; Zunger, A. *Phys. Rev. B* **1998**, *57*, 2242.
(22) Wolverton, C.; Zunger, A. *Phys. Rev. Lett.* **1998**, *81*, 606.
(23) Wolverton, C.; Zunger, A. *J. Power Sources* **1999**, *81–82*, 680.
(24) Van der Ven, A.; Aydinol, M. K.; Ceder, G.; Kresse, G.; Hafner, J. *Phys. Rev. B* **1998**, *58* (6), 2975.
(25) Ceder, G.; Van der Ven, A. *Electrochim. Acta* **1999**, *45* (1–2), 131.
(26) Arroyo y de Dompablo, M. E.; Van der Ven, A.; Ceder, G. *Phys. Rev. B* **2002**, *66*, 064112.

ture can be predicted. From this information, the complete phase diagram can be constructed.

All energies used in the parametrization are calculated with the local density approximation (LDA) to density functional theory using a plane-wave pseudopotential method as implemented in the Vienna ab initio simulation package (VASP).[27] A plane-wave basis with a kinetic energy cutoff of 400 eV was used, and reciprocal-space k-point grids between $10 \times 10 \times 4$ and $2 \times 2 \times 4$ were used (depending on the size of the supercell considered) to ensure a numerical convergence error of less than 5 meV per Li_xCoO_2 formula unit. All structures were fully relaxed. Previous calculations showed that spin polarization calculations produced a change of at most 3 meV per Li_xCoO_2 formula unit for both O3[24] and O2-Li_xCoO_2. Therefore, we performed all total-energy calculations nonpolarized.

Both O2 and O6 structures have the same triangular lattice of Li sites in a given plane, but the planes are stacked differently. The cluster expansions are constructed with four in-plane pairs, one in-plane triplet, and one inter-plane pairs for the O2 structure and with two in-plane pairs, one in-plane triplet, and two inter-plane pairs for the O6 structure. The T#2 structure has a more complex lattice, with two interpenetrating rectangular sublattices (8e and $8f_{edges}$) that can be occupied by Li. For T#2, we used nine in-plane pairs, two interplane pairs, and one triplet within the 8e sublattice; six in-plane pairs within the $8f_{edges}$ sublattice; and four in-plane pairs between the 8e and $8f_{edges}$ sites.

A least-squares fit to the total energies was used to obtain interaction parameters for the O2 and O6 structures,[28] whereas a more elaborate method based on linear programming techniques was needed for T#2 to prevent spurious ground states.[29] The cluster expansion is a crucial step in such calculations, enabling an accurate and rapid extrapolation of the total energy of any configuration from first-principles energy values of a relatively small number of configurations.[18−20]

Cells containing 1152 Li sites were equilibrated with the Monte Carlo technique for 5000 passes and sampled for 10 000 passes for O2 and O6. For the T#2 structure, up to 3600 unit cells were used. Below 600 K, convergence for T#2 was accelerated by using the n-fold Monte Carlo method,[30] which requires fewer passes: 500 equilibration passes and 1000 sampling passes were used.

As we investigate the metastable phase diagram of O2 -LiCoO₂, we restrict ourselves solely to hosts that can be derived from this structure by sheet gliding, such as O6 and T#2. Other forms of Li_xCoO_2 such as O1,[6] O3,[3] and H1−3[24,31−33] require the rearrangement of the Co−O bonds and hence are not included in our phase diagram. Nevertheless, such a transformation can occur under heat treatment,[2] so that we also restricted the construction of the phase diagram to temperatures lower than 250 °C.

3. Results and Discussion

3.1. Host Structures.

O2 Host. The O2 stacking is presented in Figure 2. Table 1 shows the calculated lattice parameters and the energies for O2-LiCoO₂ (relative to O3) and O2 CoO₂ (relative to O1). For comparison, results for the O1 and O3 hosts are also given, as these two stackings have been observed experimentally for the end members.[3,6] First-principles calculations of the relative stability of
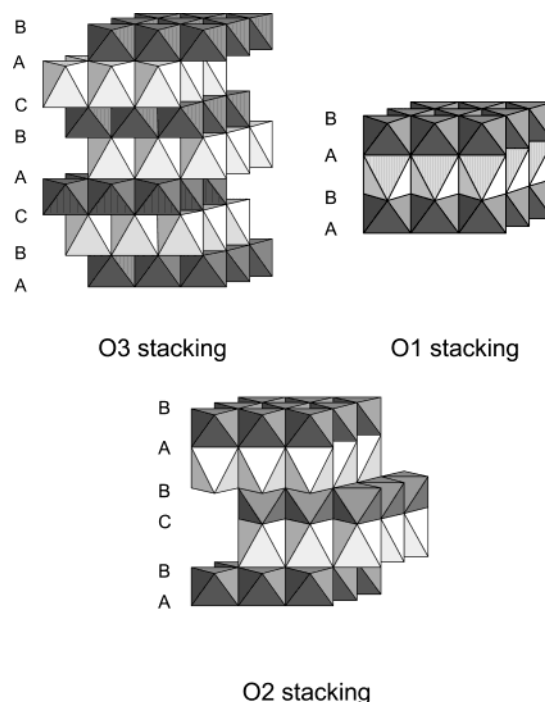
(27) Kresse, G.; Furthmuller, J. *Comput. Mater. Sci.* **1996**, *6*, 15.
(28) Connolly, J. W. D.; Williams, A. R. *Phys. Rev. B* **1983**, *27*, 5169.
(29) Garbulsky, G. D.; Ceder, G. *Phys. Rev. B* **1995**, *51*, 67.
(30) Bortz, A. B.; Kalos, M. H.; Lebowitz, J. L. *J. Comput. Phys.* **1975**, *17*, 10.
(31) Chen, Z.; Lu, Z.; Dahn, J. R. *J. Electrochem. Soc.* **2002**, *149*, 12, A1604.
(32) Croguennec, L.; Levasseur, S.; Morcrette, M.; Tarascon, J. M.; Delmas, C. Presented at the Materials Research Society (MRS) Fall Meeting, Boston, MA, Dec 2−6, 2002.
(33) Van der Ven, A.; Aydinol, M. K.; Ceder, G. *J. Electrochem. Soc.* **1998**, *145* (6), 2149.

Figure 2. O3, O2, and O1 stackings of Li_xCoO_2. The cobalt and the lithium ions are situated in the dark and light gray octahedra, respectively.

LiCoO₂ and CoO₂ in the O1 and O3 structures have previously been performed using a full potential method[24] and pseudopotentials.[21] The results given in this paper for these two stackings are consistent with those previous calculations.

As expected from LDA calculations, the calculated a_{hex} and c_{hex} cell parameters are slightly smaller than the experimental values. However, the differences in the cell parameters from O2 to O3-LiCoO₂ are in good agreement with the experimental results: O2-LiCoO₂ exhibits a smaller Co−Co (a_{hex} parameter) distance and a higher interslab distance (equal to the c_{hex} parameter divided by the number of layers used to describe the cell) (Table 1).

The energy values follow a fairly consistent pattern. For LiCoO₂, the O3 structure (Figure 2), in which the Li octahedra share only edges with the Co octahedra, has the lowest energy. Face sharing of Li and Co octahedra as in O1-LiCoO₂ (Figure 2) comes at a significant energy penalty. O2-LiCoO₂, in which Li octahedra share edges with Co octahedra on one side and faces on the other side, can be seen as intermediate between O1 and O3, as is also indicated by its energy. Therefore, in the fully lithiated material, it appears that face sharing comes at a cost of about 75 meV per face over edge sharing. For CoO₂, the situation is reversed, and face sharing is more favorable as it decreases the electrostatic interactions between the O−Co−O slabs. Indeed, the interslab distance increases as the number of shared faces decreases (Table 1). Again, the energy of O2 is nearly the average of the energies of O1 and O3, indicating that the energy is nearly proportional to the number of edge-shared octahedra.

O6 Host. We showed previously that the O6 stacking (Figure 3a) exhibits two different cobalt layers: in one layer CoO₆, octahedra share only faces with LiO₆ octahedra, whereas in the other layer, they share only

Table 1. Calculated Cell Parameters of LiCoO₂ and CoO₂ in the O1, O2, and O3 Structures[a]

	d_{Co-Co} (Å)	$d_{interslab}$ (Å)	d_{Li-O} (Å)	d_{Co-O} (Å)	interslab thickness I (Å)	slab thickness S (Å)	energy difference[b] (meV)
O1-LiCoO₂	2.765	4.731	2.09	1.893	2.697	2.034	+157
O2-LiCoO₂	2.785	4.634	2.034 × 3	1.893	2.635	1.999	+72
			2.125 × 3				
	(2.802)	(4.768)	(2.063 × 3)	(1.924 × 3)	(2.703)	(2.065)	
			(2.173 × 3)	(1.926 × 3)			
O3-LiCoO₂	2.797	4.527	2.056	1.895	2.543	1.984	0
	(2.814)	(4.683)	(2.091)	(1.921)	(2.633)	(2.049)	
O1-□CoO₂	2.779	3.995	−	1.844	2.18	1.815	0
	(2.822)	(4.293)	−	−	−	−	
O2-□CoO₂	2.786	4.088	−	1.844	2.285	1.802	+18
O3-□CoO₂	2.797	4.172	−	1.843	2.374	1.798	+39

[a] Experimental cell parameters provided in parentheses whenever available.[2,6,36] [b] Energy difference between these phases given per formula unit and referred to the most stable structures: O3 for LiCoO₂ and O1 for CoO₂
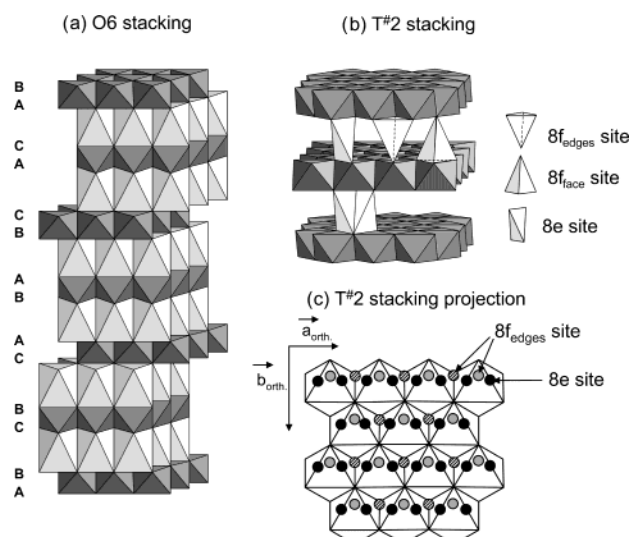

Figure 3. (a) O6 and (b) T#2 stackings of Li$_x$CoO₂. The cobalt and the lithium ions are situated in the dark and light gray polyhedra, respectively. The distorted tetrahedral sites available for the lithium ions in the T#2 structure are displayed. (c) The projection of the 8e and 8f$_{edges}$ Li sites on the [001] plane of the T#2 structure is also represented. In Figure 3c, the white octahedra represent CoO₆ below the lithium plane, the 8e sites are represented in black (they are located in the middle of the interslab space, $z = 0.25$), and the 8f$_{edges}$ are represented in light gray for the sites situated above the 8e sites displayed ($z \approx 0.27$) and in dashed circles for the sites situated below the 8e sites displayed ($z \approx 0.23$).

edges.[8,10] In these studies, the Li ions were assumed to be located in octahedral sites; therefore, the O6 name was used to describe this structure. However, the exact position of the lithium ions is not known: Li can occupy either octahedral or tetrahedral sites (one tetrahedral site shares a face with CoO₆, and the other one shares only edges). O6-Li$_{1/2}$CoO₂ and O6-Li$_{1/3}$CoO₂ were calculated considering several lithium sites and lithium/vacancy orderings. Occupation of the tetrahedral site that shares a face with CoO₆ was not considered as it was previously shown that this configuration was unfavorable in the O3 host.[34] Calculations showed that the structures with Li in octahedral sites are more stable by ∼110 meV than the stuctures with Li in the tetrahedral sites that do not share faces with CoO₆.

As a lithium-staged H1−3 structure is formed by lithium deintercalation from O3-LiCoO₂ for low Li concentrations,[24,31−33] we also considered the hypothetical formation of an O6-staged structure, with alternating empty and occupied lithium layers, in the O2-LiCoO₂ system. However, calculations showed that these staged structures were less stable than those with equal amounts of Li in every Li layer by around 55 meV. Therefore, for O6, we considered only structures with Li occupying equal numbers of octahedral sites in each layer.

T#2 Host. The T#2 stacking was recently found by Paulsen et al. for the Li$_{2/3}$Ni$_{1/3}$Mn$_{2/3}$O₂ phase.[12,13] A similar stacking is obtained after lithium deintercalation from O2 LiCoO₂ for $0.52 < x \leq 0.72$.[10] We previously reported X-ray and neutron diffraction and first-principles calculations for this structure.[10,14] Those results are only summarized here. The T#2 stacking can be described with the orthorhombic *Cmca* space group. Three distorted lithium sites are available for Li as represented in Figure 3b. Whereas the 8e sites are located in the center of the interslab space, the 8f$_{edges}$ and 8f$_{face}$ sites are slightly displaced. The projection of the 8e and 8f$_{edges}$ sites on the (a_{orth}, b_{orth}) plane is illustrated in Figure 3c. These two types of sites form interpenetrating rectangular lattices, which will be represented in our figures with solid and dashed lines, respectively, for the 8e and 8f$_{edges}$ lattices. Two types of each tetrahedral site are available per Li$_x$CoO₂ formula unit. Therefore, the filling of all 8e sites, but no 8f$_{edges}$ sites, gives a stoichiometry of Li₂CoO₂.

Calculations of the site energy at low lithium concentration indicate that the 8e site is more stable than the 8f$_{edges}$ site (that does not share any face with CoO₆ octahedra) by 15 meV and more stable than the 8f$_{face}$ site (that shares a face with a CoO₆ octahedron) by 75 meV. Therefore, the Li ions are expected to be located in the 8e sites. However, as the energy difference between the 8e and 8f$_{edges}$ sites is small compared to $k_B T_{room}$ (25 meV), some of the 8f$_{edges}$ sites might be occupied at room temperature. Therefore, structures with Li in both types of sites have to be considered in the simulation. We will reinforce this result below, showing that the phase diagram obtained by considering only the 8e site for the T#2 structure does not qualitatively agree with experiments.

3.2. Formation Energies. To parametrize the cluster expansions for the O2, O6, and T#2 hosts, the

(34) Van der Ven, A.; Ceder, G. Asta, M.; Tepesch, P. D. *Phys. Rev. B* **2001**, *64* (18), 184307.

following configurations were calculated: (a) 23 lithium/vacancy (□) configurations for the O2 structure for concentrations ranging from $x = 0$ to $x = 1$ including LiCoO₂ and □CoO₂; (b) 22 lithium/vacancy configurations for the T#2 structure with Li in the 8e site, 7 lithium/vacancy configurations for the T#2 structure with Li in the 8f$_{edges}$ site, and 10 lithium/vacancy configurations for the T#2 structure with Li distributed in both 8e and 8f$_{edges}$ types of sites (Li concentrations ranged from $x = 0$ to $x = 1$, and Li₂CoO₂ configurations with either all 8e or 8f$_{edges}$ sites filled were considered. Several Li/□ orderings were taken into account for LiCoO₂ as there are two lithium 8e (or 8f$_{edges}$) sites available per cobalt ion.); (c) 14 lithium/vacancy configurations for the O6 structure for concentrations ranging from $x = 0$ to $x = 1$ including LiCoO₂ and □CoO₂.

The formation energies of the different Li/vacancy configurations are plotted in Figure 4. We define the formation energy for a given Li/□ configuration with composition x in Li$_x$CoO₂ as

$$\Delta_f E = E - x E_{O2\text{-}LiCoO_2} - (1 - x) E_{O2\text{-}CoO_2} \qquad (1)$$

where E is the total energy of the configuration per Li$_x$□$_{1-x}$CoO₂ formula unit and $E_{O2\text{-}LiCoO_2}$ and $E_{O2\text{-}CoO_2}$ are the energies of LiCoO₂ and CoO₂, respectively, in the O2 host. The formation energy of a given structure Li$_x$CoO₂ as defined in eq 1 reflects the relative stability of that structure with respect to phase separation into fraction x of LiCoO₂ and fraction $(1 - x)$ of CoO₂.

Figure 4a shows the formation energies corresponding to structures stable with respect to phase separation into a fraction x of O2-LiCoO₂ and $(1 - x)$ of O2-CoO₂. Figure 4b shows the formation energies calculated for $x = 1$ and $x = 0$ for the three host structures. For the T#2-LiCoO₂ phase, we plot here only the lowest formation energy, which is obtained when Li occupies the 8e site in the Li/vacancy configuration shown in Figure 4b.

Several important features can be deduced from the formation energies. In agreement with experiment, the O2 structure is the more stable one for $x = 1$, with an energy 70 meV below that of T#2 and 6 meV below that of O6. For $x = 0$, the O2 and O6 stackings have approximately the same energies and are more stable than T#2 by 20 meV. For intermediate lithium concentrations, the relative stabilities of these three phases changes. For $x = \frac{1}{2}$ and $\frac{2}{3}$ (Figure 4a), T#2 is the more stable host, whereas for $x = \frac{1}{3}$, O6 is the more stable host. For $x = 0.4$, O6 is locally stable but unstable with respect to phase separation into $x = \frac{1}{3}$ and $x = \frac{1}{2}$. For $x \le 0.25$ and $x \ge 0.75$, the configurations in the O2 host are the most stable ones. Whereas the energy difference between O6 and O2 at low lithium concentration is on the order of 3 meV, which is within the numerical accuracy of the pseudopotential method, the predicted relative stability, the accuracy of which is essential for phase diagram calculations, is consistent with experiment.

3.3. Cell Parameters. The calculated interslab distances for the most stable Li/vacancy orderings are given as a function of Li concentration in Figure 5. Even if the interslab distances are calculated for ordered structures at 0 K, they can be compared with the experimental distances to verify general trends. The
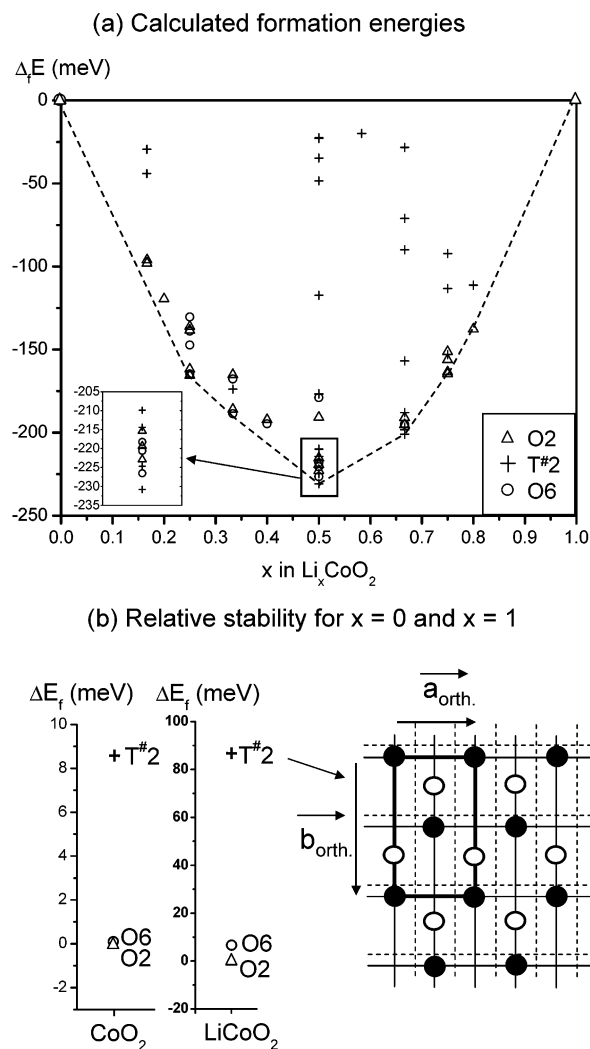

(a) Calculated formation energies

(b) Relative stability for x = 0 and x = 1

Figure 4. (a) Negative formation energies as calculated with the pseudopotential method for the different Li/vacancy arrangements considered for the O2 host (triangles), the T#2 host (crosses), and the O6 host (circles). (b) Calculated formation energies of LiCoO₂ and CoO₂ in the three hosts considered. The more stable ordering obtained for T#2-LiCoO₂ is represented on the right: the solid line and the dashed line indicate the 8e site and 8f$_{edges}$ site lattices, respectively, and the filled circles correspond to Li ions ordering in the lattice. A given in-plane ordered arrangement of Li ions can be stacked in different ways among the different Li planes. The unfilled circles designate the projection perpendicular to the Li plane of the positions of the Li ions in the adjacent Li plane.

calculated interslab distances are systematically predicted to be smaller than experimentally observed values by approximately 0.1 Å, which is typical for the local density approximation. Despite the systematic underprediction, the evolution of the calculated interslab distances is in good agreement with the observed trend: as Li is removed from O2-LiCoO₂, the O2-to-T#2 phase transition occurs and causes a large increase of the interslab distance (about 0.15 Å); then, for higher degrees of deintercalation, the interslab distance decreases while the T#2-to-O6 and O6-to-O2 phase transformations occur. However, the agreement is not as good for the O6 phases. Experimentally, the interslab distance of the O6-Li$_x$CoO₂ phases is intermediate between those of the O2 and T#2 phase, whereas it is very similar to that of the O2 phase in the first-principles calcula-
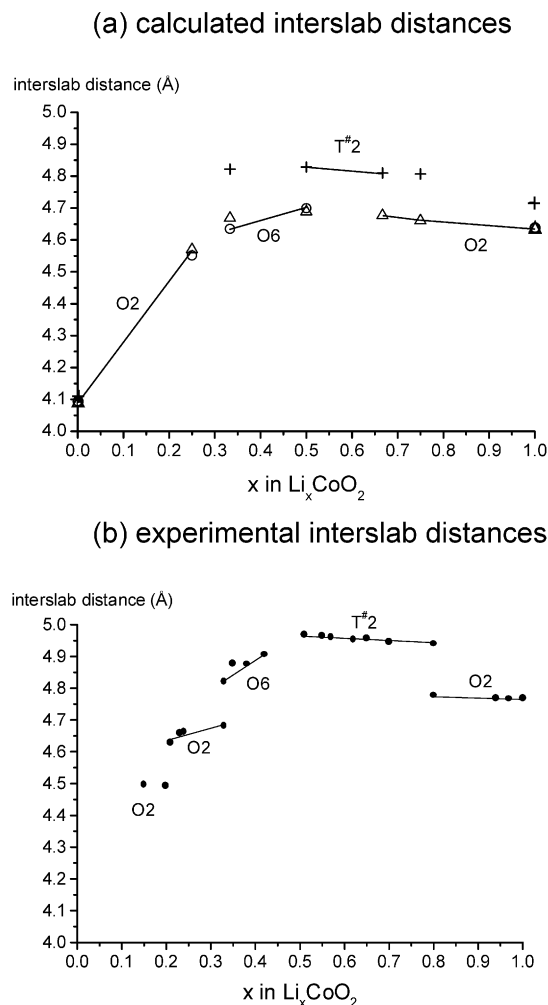
(a) calculated interslab distances

(b) experimental interslab distances

Figure 5. Comparison between the (a) calculated and (b) experimental interslab distances as a function of Li concentration. Only the calculated interslab distances for the more stable Li/vacancy orderings are given in Figure 5a for each host: O2 (triangles), $T^{\#}2$ (crosses), and O6 (circles).

tions. This could indicate that we did not consider the proper stacking and/or lithium sites for the Li_xCoO_2 phases ($0.33 \leq x < 0.42$). In the previous section, however, we showed that we tested several hypotheses for the O6 stacking. We, therefore, consider the O6 stacking as previously described in our phase diagram construction, but the existence a more complicated Li/vacancy distribution over the lithium layers is not excluded. With the exception of the O6 stacking, the good agreement between the calculated and experimental interslab distances confirms that the O2 and $T^{\#}2$ structures are the relevant ones to consider in the phase diagram calculation.

3.4. Phase Diagram. The calculated equilibrium phase diagram is represented in Figure 6. In the $T^{\#}2$ region, a large number of ordered states appeared in the Monte Carlo simulations, complicating a detailed interpretation of the results. Hence, we obtained only the approximate stability domain for the $T^{\#}2$ structure, as indicated by the dashed lines, and defer a more detailed investigation of the ordered phases for future work. However, ground states obtained by first-principles calculations for specific Li concentrations are given in the general discussion (section 3.5).
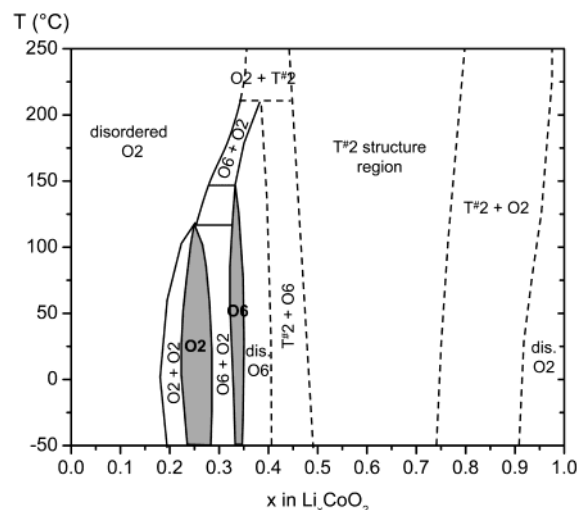

Figure 6. Partial calculated Li_xCoO_2 (O2 system) phase diagram. The dashed lines indicated the approximate limits of the $T^{\#}2$ domain. The complete phase diagram within the $T^{\#}2$ domain was not resolved. The gray areas indicate ordered phases, and the corresponding Li/vacancy orderings are given in Figure 7.
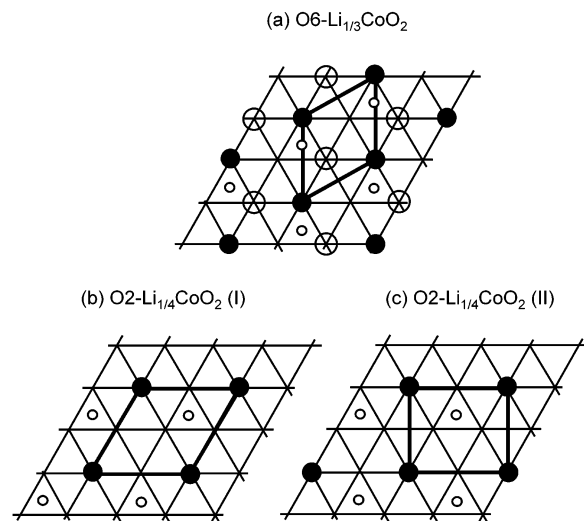
(a) $O6$-$Li_{1/3}CoO_2$

(b) $O2$-$Li_{1/4}CoO_2$ (I)   (c) $O2$-$Li_{1/4}CoO_2$ (II)

Figure 7. Ordered (a) $O6$-$Li_{1/3}CoO_2$ and (b, c) $O2$-$Li_{1/4}CoO_2$ phases found to be stable at room temperature by first-principles calculations. These structures correspond to the gray areas in Figure 6. The lattice denotes the lithium sites within a Li plane, and the filled circles correspond to Li ions. For the O2 host (b, c), the unfilled small circle denotes the projection of the Li sites of an adjacent Li plane. For the O6 host (a), the lithium positions of the two adjacent layers are different; the projection of one is represented by the small unfilled circle, and the projection of the other is represented by the large unfilled circle.

The calculated phase diagram at room temperature exhibits single-phase domains with disordered Li for $0 < x < 0.2$ (O2), $0.34 < x < 0.42$ (O6), and $0.92 < x < 1$ (O2). Ordered phases are obtained for $x = 1/4$ and $1/3$. The corresponding orderings are illustrated in Figure 7. The Li/vacancy ordering obtained for $O6$-$Li_{1/3}CoO_2$ corresponds to a $\sqrt{3} \times \sqrt{3}$ ordering in the hexagonal cell (Figure 7a). Within this ordering, a Li ion has six Li nearest neighbors at a distance of 4.80 Å. This Li/vacancy ordering is the typical ground state observed for a triangular lattice at $x = 1/3$. Indeed, it is similar to the ordering previously predicted for $O3$-$Li_{1/3}CoO_2$.[22,24]

One should note that the phase transformation from disordered O6-Li$_x$CoO$_2$ to ordered O6 Li$_{1/3}$CoO$_2$ is predicted to be second-order. The Li/vacancy ordering obtained for O2-Li$_{1/4}$CoO$_2$ corresponds to a 2×2 ordering in the triangular cell (Figure 7b). The Li−Li in-plane distance is 6×5.56 Å. Note that another orthorhombic Li/vacancy ordering (Figure 7c) was found to be only a few millielectronvolts higher in energy. Hence, some ambiguity regarding the ground state for O2-Li$_{0.25}$CoO$_2$ remains.

3.5. General Discussion.

Phase Diagram and Voltage−Composition Curve. To compare the calculations with the experimental results, it is convenient to compare the Li insertion voltage as a function of composition. The Li chemical potential, and hence the Li voltage, can be directly obtained from the Monte Carlo simulations. The voltage−composition curve contains the same information as the phase diagram for the single- or two-phase regions, but it also allows for a comparison of the the voltage-stability domains of the different phases. Figure 8a shows the calculated voltage curve of a Li//O2-LiCoO$_2$ cell at room temperature. The experimental curve is plotted again for comparison in Figure 8b. A 3.62 V average voltage is calculated for the O2-Li$_x$CoO$_2$ system. The calculated average voltage is about 0.5 V below the experimental voltage, as is typical for Li cells calculated within the LDA.[35] Nevertheless, the intercalation reaction mechanism is reflected in the shape of the voltage curve.

The agreement between the calculations and the experimental results is generally good, and the relative phase stability of the three hosts as a function of the lithium concentration is well reproduced. Basically, O2 is more stable for very high and low Li concentrations, whereas T#2 and O6 are stable for intermediate concentrations. The details of the profile obtained in the T#2 region will not be discussed here, as the cluster expansion was not accurate enough to draw conclusions on the stability of any ordered phase.

Calculations predict an ordered O6-Li$_{1/3}$CoO$_2$ phase (Figure 7a) to be stable at room temperature. The existence of this phase has not been reported. We find that the phase transition from this ordered structure to the O6 disordered structure is second-order, so that no two-phase domain exists between these phases. Hence, no flat portion is present in the voltage curve. A more careful look at the experimental voltage curve reveals some features around $x = 1/3$, as the voltage curve exhibits a small change in slope (Figure 1). This experimental observation might correspond to the formation of the ordered O6 phase.

For Li concentrations lower than $x = 1/3$, the calculated phase diagram is in quite good agreement with the experimental results, but the two-phase domain associated with the O6 → O2 phase transition is predicted to be smaller: $0.29 < x < 0.33$ instead of $0.25 \leq x < 0.33$ as observed experimentally. A specific Li ordering has not been reported near $x = 1/4$, although two different O2-Li$_x$CoO$_2$ phases were identified by XRD for $0.21 \leq x < 0.25$ and $x < 0.18$.[10] One of these phases might actually correspond to the ordered O2-Li$_{0.25}$CoO$_2$
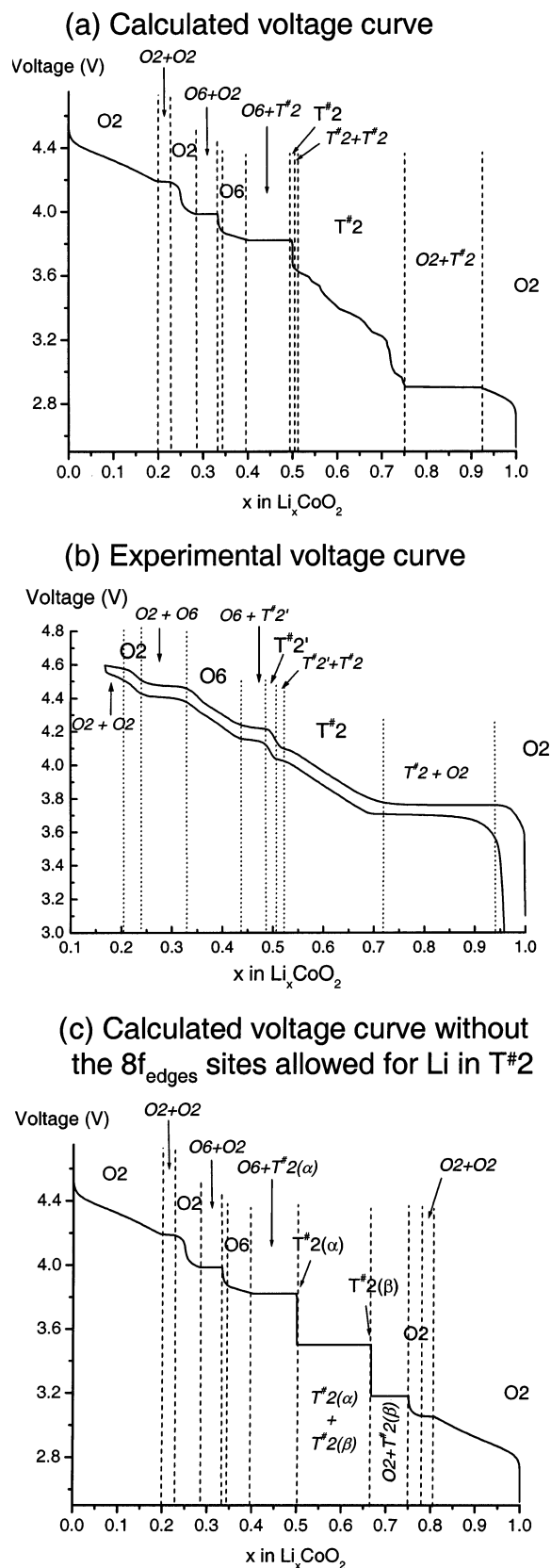
(35) Mishra, S. K.; Ceder, G. *Phys. Rev. B* **1999**, *59* (9), 6120.
(36) Levasseur, S.; Ménétrier, M.; Suard, E.; Delmas, C. *Solid State Ionics* **2000**, *128*, 11.
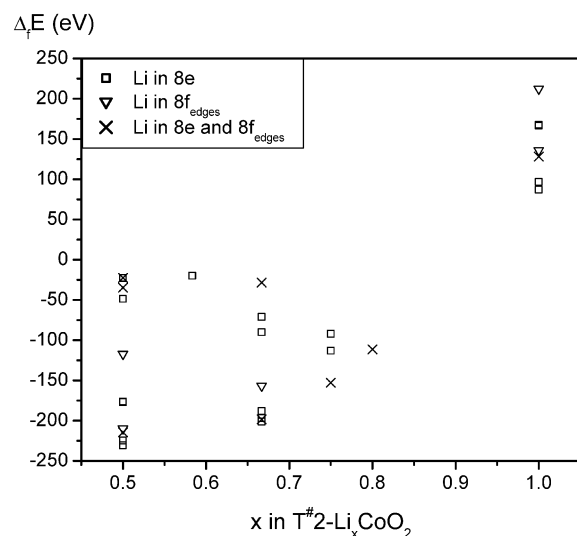
(a) Calculated voltage curve

(b) Experimental voltage curve

(c) Calculated voltage curve without the 8f$_{edges}$ sites allowed for Li in T#2

Figure 8. Calculated voltage−composition curve of a (a) Li//O2-LiCoO$_2$ cell compared to the (b) experimental curve and (c) voltage curve calculated without allowing 8f$_{edges}$ site occupation for Li ions in the T#2 structure. T#2(α) and T#2(β) correspond to the Li$_{1/2}$CoO$_2$ and Li$_{2/3}$CoO$_2$ phases, respectively, represented in Figure 10a and the left-hand side of Figure 10b. The three curves were obtained at room temperature.

Figure 9. Formation energies as calculated with the pseudo-potential method for several Li/vacancy arrangements considered for $T^\#2$ depending on the Li sites: Li only in 8e sites (squares), Li only in $8f_{edges}$ sites (triangles), and Li in both 8e and $8f_{edges}$ sites (crosses).

phase that we predict (Figure 7b and c), and the second O2 phase might correspond to the disordered $O2-Li_xCoO_2$ phase. Indeed, in the voltage curve (Figure 1), this first O2 phase exhibits a small stability domain, centered not exactly at $x = ^1/_4$ but close to this value.

$T^\#2$ structure. Even though a detailed phase diagram of the $T^\#2$ region could not be obtained, several conclusions can be made from the pseudopotential calculations. In Figure 9, we plot the formation energies of the $T^\#2$ structures with various Li/vacancy orderings in the $0.5 \leq x \leq 1$ Li concentration domain for (i) all Li in the 8e sites, (ii) all Li in the $8f_{edges}$ sites, and (iii) Li in the 8e and $8f_{edges}$ sites. For a similar Li/vacancy ordering, all of the structures with Li exclusively located in $8f_{edges}$ sites are less stable than structures with Li in 8e sites. However, it appears that structures with Li located in both 8e and $8f_{edges}$ sites can be even more stable than structures with Li located exclusively in 8e sites. This is the case, for example, for $T^\#2-Li_{0.75}CoO_2$, where the structure with Li ions in 8e and $8f_{edges}$ sites, as shown in Figure 10c, is more stable by 40 meV than structures with Li ions in 8e sites. For $T^\#2-Li_{2/3}CoO_2$, two structures [Li located in both types of sites and Li located only in 8e (Figure 10b)] are almost degenerate, as only a 3 meV energy difference is calculated. For $x = 0.5$, the more stable ordering corresponds to the structure with Li only in the more stable sites (8e) with the larger Li–Li distances, so that the electrostatic Li–Li repulsion is minimized (Figure 10a). For higher Li concentrations, placing the lithium ions in the two types of sites, 8e and $8f_{edges}$, allows the Li–Li distances to be larger than can be obtained in the structure with only 8e site occupation (for $x = ^2/_3$, the shortest Li–Li distance is given in Figure 10b), so that the higher site energy of the $8f_{edges}$ site compared to the 8e site is compensated by the reduction of Li–Li electrostatic repulsion.

Moreover, to check the importance of the $8f_{edges}$ sites of the $T^\#2$ structure, we calculated the phase diagram of the Li_xCoO_2 system allowing Li to occupy only 8e sites in $T^\#2$. The voltage curve obtained at room temperature is plotted in Figure 8c for comparison with the initial
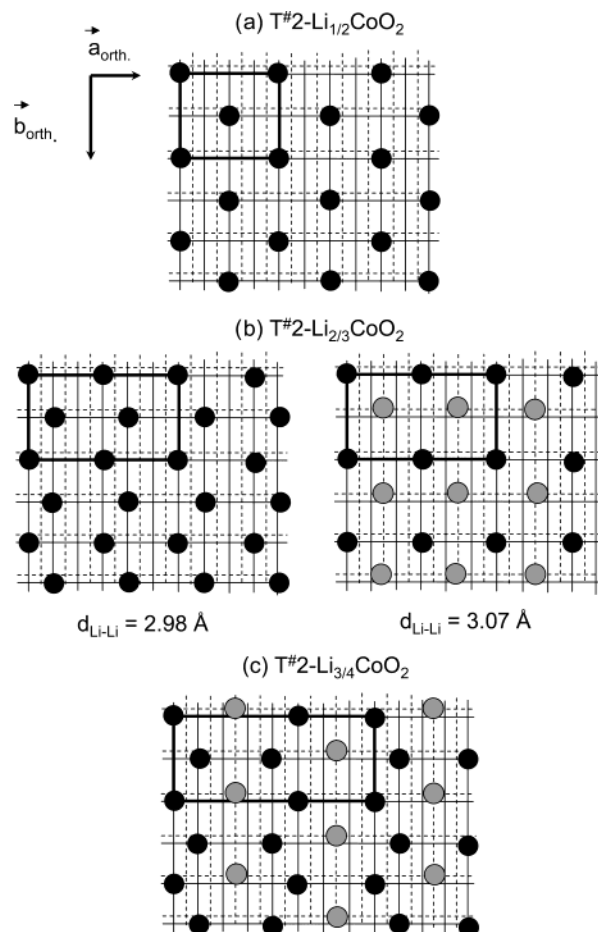

Figure 10. Li/vacancy orderings for the ground-state structures obtained for $x = ^1/_2$, $^2/_3$, and $^3/_4$ in $T^\#2-Li_xCoO_2$. The solid line and the dashed line indicate the 8e site and $8f_{edges}$ site lattices, respectively, and the black and gray circles correspond to Li ions in the 8e and $8f_{edges}$ sites, respectively. For-$T^\#2$ $Li_{2/3}CoO_2$, the two structures shown are almost degenerate, and the shortest Li–Li distance is given.

calculated curve (Figure 8a) and with the experimental one (Figure 8b). In this case, the calculated voltage curve exhibits neither the large plateau observed experimentally for $0.72 < x \leq 0.94$ nor the experimental shape of the voltage curve in the $T^\#2$ domain for $0.52 < x \leq 0.72$. In this region, two ordered phases are predicted to be stable at room temperature with stoicheometries $Li_{1/2}CoO_2$ and $Li_{2/3}CoO_2$ (Figure 10a and left-hand side of Figure 10b) that correspond to the phases labeled $T^\#2(\alpha)$ and $T^\#2(\beta)$, respectively, in Figure 8c. The artificially high stability of these structures arises because of the constraint of zero $8f_{edges}$ site occupation. The system can now choose only between order and disorder in the 8e sites, and because disorder creates too many Li–Li close neighbors, the ordered state is preferred up to higher temperatures. Allowing occupation of the $8f_{edges}$ sites creates the possibility for disorder over more sites (and hence a higher entropy) with fewer close Li–Li neighbor distances. As a result, the energy of the disordered state with 8e and $8f_{edges}$ site occupation is lower than the energy of disorder over only the 8e sites. Clearly, the $8f_{edges}$ site plays an essential role in the stability of $T^\#2$ and should be considered in both theoretical and experimental analyses of this phase.

From the relative formation energies calculated for $T^\#2$, we expect an increase in the occupation of the $8f_{edges}$ sites as the Li concentration increases from $x = 0.5$ (no $8f_{edges}$ sites occupied) to $x = 0.75$ (experimental limit of the $T^\#2$ stability). These results are in good agreement with a recent neutron diffraction study that revealed that, for $T^\#2$-$Li_{0.56}CoO_2$, the 8e sites are mainly occupied but some nuclear density is also found in the $8f_{edges}$ sites.[14] We expect neutron diffraction of a compound with a higher Li concentration to show clearly that the occupation of the $8f_{edges}$ is not negligible. In the same way, some of the $8f_{edges}$ sites might also be occupied in $T^\#2$-$Li_{2/3}Ni_{1/3}Mn_{2/3}O_2$ and $T^\#2$ $Li_{2/3}Co_{2/3}Mn_{1/3}O_2$, but calculations of the relative stabilities of the 8e and $8f_{edges}$ sites for these phases were not performed.

The ordered $T^\#2$-$Li_{0.5}CoO_2$ phase was previously called $T^\#2'$, but it was not identified because its XRD pattern is very similar to that of the $T^\#2$ phase.[10] The Li/vacancy ordering of $T^\#2$-$Li_{0.5}CoO_2$ (Figure 10a) does not imply a distortion of the orthorhombic cell, but rather a doubling of the cell in the a_{orth} direction, and therefore involves only small superstructure peaks in the $20-35°$ 2θ region. These superstructures peaks are too small compared to the noise in typical XRD patterns, so the $T^\#2'$ and $T^\#2$ phases might be difficult to distinguish experimentally.

A recent electron diffraction study[16] indicates that the large $T^\#2$ domain corresponds not to a single phase but to a series of structures with several complex Li/vacancy orderings. It was shown that, within one $T^\#2$ crystal, three $T^\#2$ superstructures could coexist in different regions: two of these correspond to $(2a_{orth} \times b_{orth} \times c_{orth})$ and $(2a_{orth} \times 2b_{orth} \times 2c_{orth})$ cells, and the other one corresponds to an incommensurate structure with $q = \gamma a^*_{orth}(\gamma = 0.23$ and $0.36)$.[16] Although we did see a tendency to form complex ordered structures in the $T^\#2$ region, more detailed work on the calculated phase diagram in the $T^\#2$ region is required to understand these observations. However, we did calculate the energies of the specific Li/vacancy orderings proposed in ref. 16 for $x = 0.75$ and did not find them to be lower than the energies of the structures in Figure 9. Given the results obtained in our current work, this seems reasonable as only the 8e sites are occupied in the proposed structures.

4. Understanding the Phase Transformations

In a previous study, it was reported that the O2 → $T^\#2$ phase transformation was associated with the nonmetal-to-metal transition.[10] A nonmetal-to-metal transition occurs in the O3-LiCoO₂ system for $x < 0.94$ and was said to be the driving force for an O3→ O3 phase transformation.[7,22,24,25] The LDA, because it is a mean-field theory for electrons, will not capture this transition, and as a result, the two-phase domain observed experimentally for $0.75 \leq x \leq 0.94$ in O3-Li_xCoO_2 does not appear in the calculated phase diagram.[24] In the calculated O2-LiCoO₂ system, the two-phase O2/$T^\#2$ region does appear, and it is not necessary to invoke a nonmetal-to-metal transition to explain this structural phase transition. The change of stacking from O2 to $T^\#2$ offers the lithium ions additional configurational entropy upon the creation of sufficient vacancies. As can be observed from the relative energies of the

different stackings at composition CoO₂ (Figure 4b), the $T^\#2$ oxygen stacking generates more O–Co–O sheet repulsion than the O2 or O6 stackings. For intermediate Li concentrations, this stacking is stabilized, as it allows the Li ions to be located in sites that do not share any faces with the CoO_6 octahedra. The Co–Li electrostatic repulsion that occurs in O2 and O6 through the common face of the Co and Li octahedra is very high for these intermediate Li concentration as some Co^{3+} are oxidized. For these intermediate Li concentrations, the unfavorable character of the 8e and $8f_{edges}$ tetrahedral sites of $T^\#2$ might therefore be compensated by the fact that they exhibit the advantage of not sharing any faces with the CoO_6 octahedra. As the number of Li ions in the interslab space decreases further, the O–Co–Co sheet repulsions once again destabilizes the $T^\#2$ host with respect to O6 and O2. Note that we do observe the O2/$T^\#2$ plateau in the calculated voltage curve, but its position is much lower than the experimental one (Figure 8a and b). Usually, LDA calculations lead to a shift of the voltage by 0.5 V, but for the plateau, a 0.8 V difference was obtained. This means that the fully lithiated state O2-LiCoO₂ is more stable in reality than is predicted by the LDA (relative to the delithiated phases at $x = 0.75$), as a more stable end member corresponds to a higher voltage. This inconsistency might be a result of the failure to predict the metal–insulator transition. Just as in the O3-Li_xCoO_2 system,[24] correctly accounting for the localized electron holes above $x = 0.95$ would lower the free energy of Li_xCoO_2 above $x = 0.95$ (it would lower the energy and also contribute extra configurational entropy because of the localized holes). This reduction in free energy above $x = 0.95$ should then increase the voltage plateau between $x = 0.75$ and 0.95, resulting in better qualitative agreement.

For the stabilization of the O6 phase, Mendiboure et al. suggested a charge ordering of Co^{3+} and Co^{4+} in the two different cobalt layers, given that, in the $R\bar{3}m$ space group of the O6 structure, two different oxygen positions describe each kind of CoO_2 layer. The trivalent cobalt ions could be mainly segregated in the sheets in which CoO_6 octahedra share faces with LiO_6, while the tetravalent cobalt would be in the other sheets,[8] thereby leading to CoO_2 slabs with different thicknesses. The O6-$Li_{0.5}CoO_2$ and O6-$Li_{0.33}CoO_2$ phases were investigated by spin-polarized calculations, but no such charge ordering was predicted. Moreover, the Co–O bonds of the two different CoO_2 slabs were found to be equivalent. Therefore, Co^{3+}/Co^{4+} ordering does not seem essential for the formation of the O6 stacking, although on the basis of LDA calculations alone, one cannot exclude the possibility that charge ordering occurs in this material.

5. Conclusions

We performed a first-principles investigation of the 0 K and finite-temperature phase stability in the O2-LiCoO₂ system with the aim of better understanding the series of unusual structures experimentally observed during Li deintercalation.

For the $T^\#2$ structure, calculations show that, even though the $8f_{edges}$ sites are less stable than the 8e sites for low Li contents, the former sites can be occupied and

are essential for the correct reproduction of the phase diagram, as they add an important amount of extra configurational entropy. We also predict several stable ordered compounds in this structure.

We indicate that what was previously thought of us as a single-phase O6 region actually consists of an ordered region near $x = {}^1/_3$ separated from a disordered phase region by a second-order phase transition. Our calculations indicate that the formation of the O6 phase is not linked to Li staging and is not driven by Co^{3+}/Co^{4+} ordering in the two different cobalt layers as previously proposed.

Finally, we predict an ordered O2 phase for $x = {}^1/_4$ and find that the O2 structure should remain stable for CoO_2 (with respect to $T^{\#}2$ and O6).

CM030002T